Title
Photochemistry in the arctic free troposphere: NOx budget and the role of odd nitrogen reservoir recycling

Journal
Atmospheric Environment, 37(24)

ISSN
1352-2310

Authors
Stroud, Craig
Madronich, Sasha
Atlas, Elliot
et al.

Publication Date
2003-08-01

DOI
10.1016/s1352-2310(03)00353-4

PERGAMON

Atmospheric Environment 37 (2003) 3351–3364

ATMOSPHERIC ENVIRONMENT

www.elsevier.com/locate/atmosenv

Photochemistry in the arctic free troposphere: NO_x budget and the role of odd nitrogen reservoir recycling

Craig Stroud[a,*], Sasha Madronich[a], Elliot Atlas[a], Brian Ridley[a], Frank Flocke[a], Andy Weinheimer[a], Bob Talbot[b], Alan Fried[a], Brian Wert[a], Richard Shetter[a], Barry Lefer[a], Mike Coffey[a], Brian Heikes[c], Don Blake[d]

[a] *Atmospheric Chemistry Division, National Center for Atmospheric Research, Boulder, CO 80301, USA*
[b] *Department of Chemistry, University of New Hampshire, Durham, NH 03824, USA*
[c] *School of Oceanography, University of Rhode Island, Narragansett, RI 02881, USA*
[d] *Department of Chemistry, University of California, Irvine, CA 92697, USA*

Received 22 December 2002; accepted 30 April 2003

Abstract

The budget of nitrogen oxides (NO_x) in the arctic free troposphere is calculated with a constrained photochemical box model using aircraft observations from the Tropospheric O_3 Production about the Spring Equinox (TOPSE) campaign between February and May. Peroxyacetic nitric anhydride (PAN) was observed to be the dominant odd nitrogen species (NO_y) in the arctic free troposphere and showed a pronounced seasonal increase in mixing ratio. When constrained to observed acetaldehyde (CH_3CHO) mixing ratios, the box model calculates unrealistically large *net* NO_x losses due to PAN formation (62 pptv/day for May, 1–3 km). Thus, given our current understanding of atmospheric chemistry, these results cast doubt on the robustness of the CH_3CHO observations during TOPSE. When CH_3CHO was calculated to steady state in the box model, the *net* NO_x loss to PAN was of comparable magnitude to the *net* NO_x loss to HNO_3 (NO_2 reaction with OH) for spring conditions. During the winter, *net* NO_x loss due to N_2O_5 hydrolysis dominates other NO_x loss processes and is near saturation with respect to further increases in aerosol surface area concentration. NO_x loss due to N_2O_5 hydrolysis is sensitive to latitude and month due to changes in diurnal photolysis (sharp day–night transitions in winter to continuous sun in spring for the arctic). Near NO_x sources, HNO_4 is a *net* sink for NO_x; however, for more aged air masses HNO_4 is a *net* source for NO_x, largely countering the NO_x loss to PAN, N_2O_5 and HNO_3. Overall, HNO_4 chemistry impacts the timing of NO_x decay and O_3 production; however, the cumulative impact on O_3 and NO_x mixing ratios after a 20-day trajectory is minimal.

Keywords: Atmospheric chemistry; Arctic troposphere; TOPSE; Peroxynitric acid; Acetaldehyde

1. Introduction

Nitrogen oxides ($NO_x = NO + NO_2 + NO_3$) play a critical role in the oxidizing capacity of the troposphere through their impact on the production, loss and partitioning of radical species (OH, HO_2 and RO_2) (Levy II, 1972; Crutzen, 1974, 1979). Furthermore, NO_x not only affects the concentration and partitioning of radical species, but also directly participates in the reactions leading to the production and distribution of ozone (O_3), i.e. reactions of peroxy radicals with nitric oxide (Chameides and Walker, 1973). Sources of NO_x in the free troposphere include convective transport from surface sources, lightning, stratospheric injection, aircraft emissions and recycling reactions from reactive odd nitrogen reservoir species such as nitric acid (HNO_3) and

*Corresponding author. Tel.: +1-303-497-1449; fax: +1-303-497-1477.
E-mail address: cstroud@ucar.edu (C. Stroud).

1352-2310/03/$ - see front matter
doi:10.1016/S1352-2310(03)00353-4

peroxyacetic nitric anhydride (PAN) (Roberts, 1990; Jacob et al., 1996; Levy II et al., 1999). A 3-D modeling study by Moxim et al. (1996) showed that the magnitude and seasonal cycle of the global tropospheric integral of NO_x are barely affected by the inclusion of PAN chemistry; the global emissions of NO_x balance formation of HNO_3. However, as pointed out by Moxim et al. reservoir species such as PAN can regionally provide an efficient mechanism for redistributing the NO_x far from source regions, and thus can perturb regional O_3 photochemistry. As an illustration, Moxim et al. estimate that PAN decomposition can increase the monthly mean NO_x mixing ratios in the remote lower troposphere over the North Atlantic and North Pacific by a factor of 5.

Direct measurements of total reactive odd nitrogen (NO_y) and its suspected dominant components (NO_x, HNO_3, PAN) show good agreement at most continental sites at ppbv levels, i.e. components comprise greater than 90% of observed NO_y (Parrish et al., 1993; Sandholm et al., 1994). At remote locations, NO_y measurements and the NO_y sum have disagreed by 30–50% (Ridley, 1991; Atlas et al., 1992; Crosley, 1996; Kondo et al., 1997); however the recent SONEX study in the North Atlantic upper troposphere showed that the sum of the speciated NO_y could account for greater than 90% of measured NO_y (Talbot et al., 1999). Modeled peroxynitric acid (HNO_4) accounted for the majority of the remaining NO_y speciation.

In this study, we quantify the NO_x budget in the arctic free troposphere during the Tropospheric O_3 Production about the Spring Equinox (TOPSE) 2000 campaign using a chemical box model constrained by aircraft observations. The major goal of TOPSE was to study the late winter-to-spring transition in arctic photochemistry in order to assess the importance of the springtime increase in tropospheric photochemical O_3 production with regard to the observed springtime maximum in high-latitude tropospheric O_3. In this remote environment, it is expected that convection, lightning and aircraft sources of NO_x are minimal so that recycling reactions from reservoir species dominate the NO_x production and loss. Observations of the partitioning of the NO_y species in the arctic free troposphere are sparse. Knowing the distribution of NO_y and how recycling reactions redistribute NO_y in the arctic free troposphere indicates whether the arctic free troposphere simply transports NO_x as PAN or whether the arctic free troposphere is a region of permanent removal of odd nitrogen from the global atmosphere as HNO_3. If a large fraction of the NO_x accumulates as PAN in the arctic free troposphere, then subsequent episodic transport of these air masses to mid-latitudes along subsiding trajectories would provide large sources of NO_x which could shift the O_3 budget to *net* O_3 production in impacted regions (Beine et al., 1997; Hamlin and Honrath, 2002). Here, we also explore the importance of other reactive odd nitrogen species, such as N_2O_5 and HNO_4, which rapidly inter-convert with NO_x on intermediate time scales (on the order of a day), and thus impact how efficiently NO_x is converted to either PAN or HNO_3 in arctic air masses.

2. Model description

2.1. Data sorting

The TOPSE campaign was composed of a series of seven round-trip deployments between 4 February 2002 and 23 May 2002 with missions generally sampling the mid-to-high latitude troposphere over North America in the corridor originating in Colorado, traversing over Manitoba and Hudson Bay before ending north of Greenland and returning back to Colorado. A C-130 aircraft was used to probe the composition of the troposphere between 0 and 8 km. We based our analysis on a merged time series of the aircraft observations where the measurements were averaged over a common time interval of 1 min. We sorted the observations based on latitude (40–50°N, 50–58°N, 58–85°N), altitude (0–1, 1–3, 3–6, 6–8 km) and month (2 February deployments, 2 March deployments, 2 April deployments, 1 May deployment) and derived statistics (mean, 1σ standard deviation about the mean, median) for sorted cases. Tables 1 and 2 list statistics for many of the critical chemical species over the springtime transition in the arctic (58–85°N), separated for the 1–3 and 3–6 km altitude layers. Descriptions of the analytical measurement techniques and references can be found in a TOPSE overview paper (Atlas et al., 2003). Canister-GC/MS measurements of CH_3CHO were performed, but mixing ratios are considered preliminary (D. Blake, personal communication) because canister sampling for CH_3CHO has not been validated (factor of two uncertainty). Interestingly, prior informal comparisons between canister and airborne in situ CH_3CHO measurements during PEM-Tropics-B (Singh et al., 2001) and Trace-P showed significant point-by-point variability, but overall reasonable agreement for median values.

2.2. Model approach

Our general approach in quantifying the NO_x budget was to calculate 24-h average NO_x production and loss rates for odd nitrogen recycling reactions for different months and altitudes by using a photochemical box model constrained by the measured medians listed in Tables 1 and 2. The photochemical box model was run for repetitive diurnal solar cycles to diel steady state with photolysis frequencies (j values) calculated using

Table 1
Statistics generated from sorted aircraft data in the arctic mid-troposphere (58–85°N, 3–6 km)

Parameter	February		March		April		May	
	Mean ± std.	Median	Mean ± std.	Median	Mean ± std.	Median	Mean ± std.	Median
Latitude (°)	65 ± 5	64	71 ± 8	71	71 ± 8	72	71 ± 7	73
Altitude (km)	5.1 ± 0.8	5.5	5.0 ± 0.9	5.4	5.0 ± 0.8	5.1	4.8 ± 0.9	5.2
Temperature (K)	237 ± 8	236	239 ± 8	238	238 ± 7	237	246 ± 8	243
Water vapor (g/kg)	0.23 ± 0.33	0.08	0.29 ± 0.37	0.15	0.22 ± 0.24	0.14	0.32 ± 0.47	0.19
$j(O^1D)$ (/s)	$9 \pm 7 \times 10^{-7}$	7×10^{-7}	$3 \pm 3 \times 10^{-6}$	3×10^{-6}	$6 \pm 5 \times 10^{-6}$	6×10^{-6}	$1.3 \pm 0.7 \times 10^{-5}$	1.2×10^{-5}
Surface Albedo	0.82 ± 0.08	0.84	0.87 ± 0.03	0.87	0.84 ± 0.06	0.85	0.77 ± 0.09	0.78
Cloud Factor	0.93 ± 0.19	0.98	0.97 ± 0.16	1.01	0.96 ± 0.07	0.97	0.95 ± 0.07	0.95
O_3 (ppbv)	55 ± 7	54	63 ± 13	60	67 ± 10	65	75 ± 11	78
NO_x (pptv)	20 ± 16	18	25 ± 22	21	17 ± 13	15	30 ± 13	30
PAN (pptv)	117 ± 37	111	199 ± 96	177	263 ± 195	222	319 ± 86	323
HNO_3 (pptv)	39 ± 24	34	58 ± 70	32	51 ± 57	37	76 ± 42	68
$RONO_2$ (pptv)[a]	24 ± 2.2	24	28 ± 7.6	24	20 ± 2.8	20	11 ± 1.4	10
NO_y (pptv)	283 ± 89	279	352 ± 150	326	385 ± 234	332	436 ± 112	446
NO_y Deficit (pptv)[b]	60 ± 53	73	1.5 ± 54	37	4.2 ± 59	11	−18 ± 43	−3
CH_4 (ppmv)	1.81 ± 0.01	1.81	1.83 ± 0.02	1.83	1.83 ± 0.01	1.86	1.83 ± 0.01	1.82
CH_2O (pptv)	100 ± 88	90	91 ± 92	73	47 ± 82	41	64 ± 68	55
H_2O_2 (pptv)	82 ± 81	58	115 ± 77	105	165 ± 67	168	180 ± 74	174
CH_3OOH (pptv)	113 ± 113	72	184 ± 121	157	126 ± 66	120	130 ± 64	125
CO (ppbv)	145 ± 11	146	154 ± 12	151	154 ± 9	154	145 ± 10	147
C_3H_8 (pptv)	589 ± 156	543	626 ± 255	607	398 ± 121	397	186 ± 43	179
CH_3CHO (pptv)	112 ± 42	104		140[c]	165 ± 101	141	183 ± 97	160
$CH_3C(O)CH_3$ (pptv)	381 ± 98	382		550[c]	692 ± 218	674	860 ± 214	839

[a] $RONO_2$ included methyl, ethyl, 1-propyl, 2-propyl, and 2-butyl nitrate.
[b] Only coincident data considered. Mean $RONO_2/NO_y$ ratio applied to NO_y observations to expand $RONO_2$ database.
[c] A highly uncertain value due to lack of data.

radiative transfer code (TUV Version 4; (Madronich and Flocke, 1998)). The TUV module was initialized for the various cases with measured median values for latitude, Julian day, altitude, O_3 column and albedo. Cloud correction factors were calculated by comparing the TUV clear-sky results run on individual aircraft points and individual j value measurements. Median values of the sorted cloud correction factors were then applied to all the j values calculated by TUV within the photochemical box model. The median $j(NO_2)$ and $j(O^1D)$ cloud correction factor ranged between 0.82–1.06 and 0.92–1.00, respectively, for the arctic free troposphere sampled during TOPSE. The TUV module was updated with cross section and quantum yields from recent evaluations for inorganic species (DeMore, 1997, 2000) and organic species (Atkinson, 1997b; Atkinson et al., 2000). The photodissociation of HNO_4 in the near-IR was incorporated into TUV based on the recent measurements of Roehl et al. (2002). The clear sky photodissociation rate for HNO_4 is on the order of $10^{-5}\,s^{-1}$ at 240 K, largely invariant with changes in solar zenith angle.

NCAR's master mechanism was used as the chemical scheme within the model (Madronich and Calvert, 1990). The inorganic chemistry has undergone updates since then with the most recent recommendations taken from (DeMore, 1997, 2000). The hydrocarbon chemistry in the master mechanism is treated explicitly and includes the photo-oxidation of partly oxygenated organic species. Alkanes up to C_8, alkenes up to C_3 and aromatics up to C_8 were observed in the arctic free troposphere and were considered as initial hydrocarbon reagents in the gas-phase mechanism. The chemistry of the methyl peroxy radical is treated explicitly; a counter scheme is used for the other organic peroxy radicals (Madronich and Calvert, 1990). The rate coefficients for organic peroxy radical reactions were updated based on recent recommendations (Tyndall et al., 2001; Mereau et al., 2000). Alkoxy radical reactions were also updated based on the latest DeMore et al. recommendation (for CH_3O) and the specific studies in Atkinson (1997a) and Mereau et al. for the larger alkoxy radicals. Rate coefficients for hydrocarbons reactions with OH were updated based on the latest JPL compilations (DeMore, 1997, 2000) and the Atkinson (1994) review. The OH-initiated ethene oxidation mechanism was modified to include multiple branching for the β-hydroxy ethoxy radical reaction with NO (Orlando et al., 1998). OH-initiated rate coefficients for oxygenated hydrocarbons were updated from the Atkinson (1994) compilation.

Table 2
Statistics generated from sorted aircraft data in the arctic lower free troposphere (58–85°N, 1–3 km)

Parameter	February		March		April		May	
	Mean ± std.	Median	Mean ± std.	Median	Mean ± std.	Median	Mean ± std.	Median
Latitude (°)	67 ± 7	65	70 ± 9	74	68 ± 8	68	69 ± 9	72
Altitude (km)	2.0 ± 0.6	2.1	2.1 ± 0.6	2.2	2.1 ± 0.6	2.1	1.9 ± 0.5	1.8
Temperature (K)	252 ± 7	249	255 ± 8	253	258 ± 7	256	264 ± 5	266
Water vapor (g/kg)	0.68 ± 0.81	0.43	1.0 ± 1.1	0.57	0.89 ± 0.79	0.70	1.0 ± 0.6	0.93
$j(O^1D)$ (/s)	$4 \pm 4 \times 10^{-7}$	3×10^{-7}	$3 \pm 3 \times 10^{-6}$	2×10^{-6}	$6 \pm 5 \times 10^{-6}$	6×10^{-6}	$1 \pm 1 \times 10^{-5}$	1×10^{-5}
Surface Albedo	0.82 ± 0.08	0.84	0.87 ± 0.03	0.87	0.86 ± 0.06	0.86	0.78 ± 0.10	0.79
Cloud Factor	0.94 ± 0.16	0.98	0.96 ± 0.15	1.01	0.97 ± 0.14	1.00	0.96 ± 0.16	1.01
O_3 (ppbv)	46 ± 4	45	53 ± 5	53	55 ± 6	54	56 ± 12	57
NO_x (pptv)	11 ± 15	7	25 ± 30	15	18 ± 17	13	28 ± 17	27
PAN (pptv)	158 ± 135	117	210 ± 106	197	199 ± 83	170	195 ± 98	172
HNO_3 (pptv)	69 ± 230	34	65 ± 61	39	81 ± 80	52	103 ± 52	96
$RONO_2$ (pptv)[a]	31 ± 7.8	27	31 ± 5.3	28	21 ± 2.9	21	11 ± 0.9	11
NO_y Deficit (pptv)[b]	34 ± 50	35	−30 ± 59	11	−39 ± 52	−32	−56 ± 55	−66
NO_y (pptv)	301 ± 168	255	342 ± 161	310	309 ± 137	272	294 ± 142	265
CH_4 (ppmv)	1.84 ± 0.02	1.84	1.84 ± 0.01	1.84	1.84 ± 0.01	1.84	1.83 ± 0.01	1.83
CH_2O (pptv)	143 ± 160	106	166 ± 193	91	121 ± 150	48	93 ± 71	84
H_2O_2 (pptv)	45 ± 58	12[c]	152 ± 118	124	261 ± 151	235	340 ± 209	314
CH_3OOH (pptv)	94 ± 108	70	145 ± 78	140	187 ± 103	168	253 ± 115	251
CO (ppbv)	164 ± 19	161	156 ± 11	153	156 ± 5	156	144 ± 8	144
C_3H_8 (pptv)	920 ± 248	909	806 ± 176	780	448 ± 162	464	175 ± 43	166
CH_3CHO (pptv)	122 ± 43	107	153 ± 69	138	155 ± 61	140	218 ± 140	205
$CH_3C(O)CH_3$ (pptv)	426 ± 164	385	543 ± 203	502	621 ± 170	582	772 ± 140	732

[a] $RONO_2$ included methyl, ethyl, 1-propyl, 2-propyl, and 2-butyl nitrate.
[b] Only coincident data considered. Mean $RONO_2/NO_y$ ratio applied to NO_y observations to expand $RONO_2$ database.
[c] Half the estimated detection limit.

The kinetics of the HO_2 self-reaction were recently measured (Christensen et al., 2002) to be lower than the current recommendation. As discussed by Stroud et al. (2003), the impact of these new data on HO_2, H_2O_2 and CH_3OOH mixing ratios was not significant for TOPSE conditions.

3. Results and discussion

3.1. Lifetime considerations for odd nitrogen species in the arctic free troposphere

In the remote troposphere, NO_x is observed to be a small fraction of the total oxidized nitrogen budget due to the rapid processing of NO_x to its reservoir species during transport from NO_x sources. Fig. 1 illustrates the seasonal changes in lifetimes for odd nitrogen species in the arctic middle troposphere (3–6 km). Actual median latitudes and altitudes used in the TUV calculations are shown in Tables 1 and 2. NO_x has a lifetime less than a week in the arctic free troposphere. The increase in photochemical activity between February and May results in the NO_x lifetime decreasing from 6 to 2 days. In contrast, PAN and HNO_3 are more stable species with lifetimes on the order of a month (May) to a year

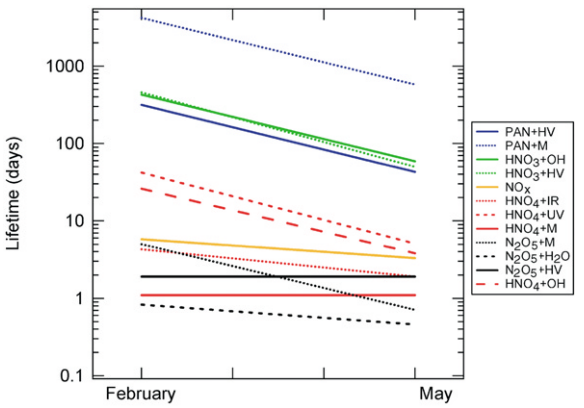

Fig. 1. Seasonal trend in lifetimes of reactive odd nitrogen species in the 3–6 km layer. The plot was created from points for February and May conditions and linearly interpolated. Lifetimes calculated with median latitudes for February (64°N, day–night j profiles) and May (73°N, smoother j diurnal profiles). Photolysis rates were diurnally averaged to calculate lifetimes. N_2O_5 chemistry is strongly dependent on median latitude.

(February). PAN photolysis dominates PAN thermal decomposition in the arctic middle troposphere, while OH oxidation and photolysis contribute comparably to

HNO_3 loss. Median temperatures in the arctic mid-troposphere showed little change between winter and spring (from 237 to 243 K); as a result, PAN thermal decomposition changes were small. HNO_4 and N_2O_5 have shorter lifetimes, comparable in magnitude to NO_x. HNO_4 thermal decomposition and IR photolysis are the important loss mechanisms for HNO_4 in the arctic free troposphere. Our calculations result in IR photodissociation contributing 20% and 37% to the total HNO_4 loss in February and May, respectively. Hydrolysis is the most important loss process for N_2O_5 throughout the winter to spring transition. N_2O_5 photolysis does make a smaller but important contribution in the winter (sensitive to February median latitude). Similarly, N_2O_5 thermal decomposition makes an important contribution in the spring (sensitive to May median temperature). The steady-state assumption should be a reasonable approximation for HNO_4 and N_2O_5 considering both have relatively short lifetimes and given the remote location of the observations. However, PAN and HNO_3 mixing ratios are likely impacted by chemistry as well as transport.

3.2. Observed seasonal trends in individual NO_y species mixing ratios

Fig. 2 presents the observed seasonal dependence to the partitioning of the NO_y budget in the lower (1–3 km, panel a) and middle (3–6 km, panel b) free troposphere. Mean mixing ratios with measurement uncertainties are shown for months between February and May with all the observations north of 58°. Table 3 lists how the measurement uncertainties were estimated for each of the odd nitrogen species (columns 1 and 2). The mean NO_x mixing ratios show a weak seasonal increase from February to May in both altitude ranges (from 11 to 28 pptv for 1–3 km; from 20 to 30 pptv for 3–6 km). Surface measurements at Zeppelin mountain, Svalbard (78°N, 11°E, 474 m asl) generally ranged between 10 and 40 pptv with no apparent seasonal trend between February and May (Beine et al., 1996). Surface measurements by Beine et al. (1997) at Poker Flat, Alaska showed a weak NO_x trend with daytime NO medians increasing from 5 to 15 pptv between March and May. These other surface observations are similar in magnitude and trend to the TOPSE observations. Thus, the TOPSE observations reinforce our understanding of the temporal NO_x distribution near the surface while enhancing our understanding of the vertical and spatial NO_x distribution.

The mixing ratios of the reservoir species, PAN and HNO_3, show a strong upward seasonal trend, with PAN showing the largest increase from a mean value of 117 pptv in February to 319 pptv in May for the 3–6 km layer. HNO_3 increased from 39 to 76 pptv over this time period while PPN showed no significant seasonal trend

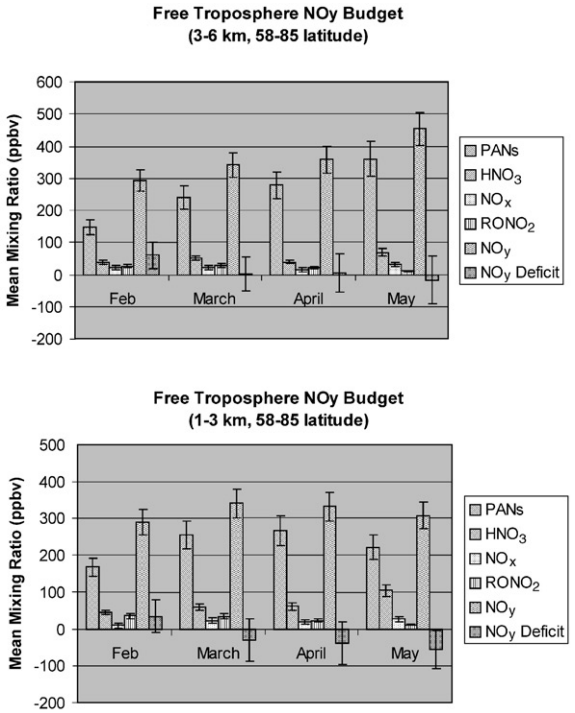

Fig. 2. Monthly evolution of measured mean mixing ratios for reactive odd nitrogen species in the 3–6 km layer (panel a) and 1–3 km layer (panel b) between 58°N and 85°N. Only coincident data was used to generate means. Mean $RONO_2$/NO_y ratio was applied to NO_y observations to expand $RONO_2$ database. Limits represent measurement uncertainties.

Table 3
Measurement uncertainties for odd nitrogen species and the median February (3–6 km) NO_y deficit

Species	Measurement uncertainty	Mixing ratios for median NO_y deficit point (in pptv)	Uncertainty (in pptv)
NO	2 pptv + 5% (1 min)	5	2
NO_2	4 pptv + 5% (1 min)	9	5
PANs	15%	125	19
HNO_3	15%	66	9.9
$RONO_2$	20%	17	3.4
NO_y	5 pptv + 10% (1 min)	286	34
NO_y Deficit		64[a]	41[b]

[a] Calculated from the median of $[NO_y]$–$[NO_x]$–[PANs]–$[HNO_3]$–$[RONO_2]$ coincident points.

[b] Calculated from the sum of uncertainties in column added in quadrature.

with mean mixing ratios between 32 and 35 pptv in the 3–6 km layer. The pronounced seasonal increase in PAN and HNO_3 in Fig. 2 is an indication of the springtime growth in photochemical activity. The observed increase in PAN mixing ratios is consistent with the weak seasonal increase in observed CH_3CHO and NO_x mixing ratios, the strong seasonal trend in observed OH and the persistence of cold temperatures (long PAN thermal decomposition lifetime). Changes in transport also play a role as supported by the concurrent increase in NO_y. Similar trends were seen for PAN and HNO_3 in the lower free troposphere (panel 2b) with the exception of the decrease in PAN between April and May. This is likely a reflection of the significant warming trend (median $T = 256-266$ K) between April and May in the 1–3 km layer.

3.3. *In situ NO_x cycling in the arctic free troposphere*

3.3.1. *Introduction*

Numerous studies have examined the role of NO_y reservoir species in NO_x recycling in remote environments (Schultz et al., 2000; Jacob et al., 1996; Kotchenruther et al., 2001; Hamlin and Honrath, 2002). The importance of HNO_3 and PAN as a sink/source for NO_x has been observed to vary with season and location. For example, during SUCCESS in the upper troposphere over the US, HNO_3 was the dominant NO_y species and the principal sink for NO_x (Jaegle et al., 2000). Similarly, over the North Atlantic during SONEX, HNO_3 composed the largest fraction of NO_y (median ratio of 0.35) in the upper troposphere (Talbot et al., 1999). In urban areas, PAN is a net sink for NO_x (Roberts et al., 2002); however, in remote areas PAN has been calculated to be a net source for NO_x. For example, Schultz et al. (1999) showed that the NO_x responsible for O_3 production within the South Pacific below 4 km can largely be explained by the decomposition of PAN transported into the region from biomass burning plumes at higher altitudes. Kotchenruther et al. (2001) showed that PAN decomposition contributed significantly to NO_x mixing ratios in the eastern Pacific troposphere off the coast of the US, especially for subsiding air masses originating from Asia. Hamlin and Honrath (2002) also showed that springtime NO_x in air masses transported from the arctic to the North Atlantic can largely be attributed to PAN decomposition along the subsiding trajectories. The common feature among these studies is enhanced levels of PAN in the upper troposphere (from biomass burning convection, from Asian outflow convection and arctic wintertime accumulation) followed by decomposition and release of NO_x along subsiding trajectories.

From our modeling analysis, we address the in situ partitioning of NO_x to its oxidized products in the arctic free troposphere. Tables 4 and 5 present the 24-h average NO_x budget in the arctic free troposphere due to localized reservoir recycling in the 3–6 and 1–3 km layers. *Net* NO_x fluxes were calculated from constrained box model simulations run to steady state where NO_x,

Table 4
24-h average NO_x budget in the arctic free troposphere due to reservoir cycling (3–6 km)

Reactions considered	February	March	April	May
$OH + NO_2 \rightarrow HNO_3$ $HNO_3 + OH \rightarrow H_2O + NO_3$ $HNO_3 + h\nu \rightarrow OH + NO_2$	−0.5	−1.2	−0.8	−4.4
$CH_3CO_3 + NO_2 \rightarrow PAN$	−3.4[a]	−8.6[a]	−9.3[a]	−31[a]
$PAN + M \rightarrow CH_3CO_3 + NO_2$ $PAN + h\nu \rightarrow CH_3CO_3 + NO_2$	−0.5[b]	−1.1[b]	−1.0[b]	−3.8[b]
$NO_2 + NO_3 \rightarrow N_2O_5$ $N_2O_5 + M \rightarrow NO_2 + NO_3$ $N_2O_5 + h\nu \rightarrow NO_2 + NO_3$	−2.9	−2.0	−0.9	−0.05

A negative value indicates net NO_x loss (pptv/day). Species constrained at measured medians.
Calculated from the 5th day of a constrained box model simulation (fixed NO_x, HNO_3 and PAN at measured medians). Model run at observed monthly median latitudes of 64°N, 71°N, 72°N, and 73°N.
[a] Model was constrained by estimated median CH_3CHO measurement.
[b] Model calculated CH_3CHO to steady state.

Table 5
24-h average NO_x budget in the arctic free troposphere due to reservoir cycling (1–3 km)

Reactions considered	February	March	April	May
$OH + NO_2 \rightarrow HNO_3$ $HNO_3 + OH \rightarrow H_2O + NO_3$ $HNO_3 + h\nu \rightarrow OH + NO_2$	−0.1	−0.8	−1.1	−7.0
$CH_3CO_3 + NO_2 \rightarrow PAN$	−2.5[a]	−7.4[a]	−14[a]	−62[a]
$PAN + M = CH_3CO_3 + NO_2$ $PAN + h\nu \rightarrow CH_3CO_3 + NO_2$	−0.4[b]	−0.7[b]	−1.2[b]	−2.2[b]
$NO_2 + NO_3 \rightarrow N_2O_5$ $N_2O_5 + M \rightarrow NO_2 + NO_3$ $N_2O_5 + h\nu \rightarrow NO_2 + NO_3$	−1.8	−4.5	−2.1	−0.1

A negative value indicates net NO_x loss (pptv/day). Species constrained at measured medians.
Calculated from the 5th day of a constrained box model simulation (fixed NO_x, HNO_3 and PAN at measured medians). Model run at observed monthly median latitudes of 65°N, 74°N, 68°N, and 72°N.
[a] Model was constrained by estimated median CH_3CHO measurement.
[b] Model calculated CH_3CHO to steady state.

PAN and HNO_3 were fixed at measured medians. In these simulations, hydrocarbons, CH_4, CO, O_3, H_2O, CH_2O, H_2O_2 and CH_3OOH were also constrained at their measured medians. Two simulations were performed for Tables 4 and 5, with CH_3CHO either fixed at its measured median or calculated. Two simulations were necessary due to significant model-measurement differences for CH_3CHO. The following section summarizes the model results with CH_3CHO constrained, while the remainder of the paper relies on CH_3CHO calculated from the model photochemistry.

3.3.2. In situ NO_x cycling with acetaldehyde constrained

Modeled steady-state CH_3CHO in the arctic free troposphere underestimated observations by an order of magnitude for all months during the campaign. For example, in May, modeled steady-state CH_3CHO underestimated observations by a factor of 20 (measured 160 pptv vs. model 8 pptv). Tables 4 and 5 illustrate that constraining CH_3CHO in the model results in a *net* NO_x loss to PAN dominating other NO_x chemical losses for all months and altitude ranges. However, a closer inspection of the *net* NO_x loss to PAN suggests the magnitudes are unrealistically large. For example, in May, *net* NO_x loss rates are calculated as large as -31 and -62 pptv/day for 3–6 and 1–3 km, respectively. Given that NO_x median mixing ratios in May are 27 and 30 pptv for the 3–6 and 1–3 km, the NO_x loss rates would imply significant regional sources of NO_x in the arctic free troposphere. While some localized NO_x sources are possible, at times, due to lightning or aircraft emissions, it does not seem feasible that for median conditions, over wide regions of the arctic free troposphere, there are NO_x sources of this magnitude. Similarly, these *net* PAN production rates imply that in a relatively short time period air masses in the arctic may have significantly more PAN than observed. For example, a 5-day simulation using constrained CH_3CHO resulted in an enhancement of modeled PAN by 67% from its initial median measured mixing ratio (323–539 pptv).

Several arguments may be postulated to explain these model-measurement differences for CH_3CHO: (1) widespread surface emissions (Domine and Shepson, 2002) and efficient transport into the arctic free troposphere, (2) incomplete distribution of measured hydrocarbons and an initialization of reactive hydrocarbons at observed values instead of some representative concentration along the arrival trajectory, (3) incomplete understanding of model organic oxidation pathways, (4) CH_3CHO artifact formation during sampling procedures or other instrumental errors. However, upon further inspection, several of these postulates should be discarded. In May, the CH_3CHO lifetime due to photolysis and OH reaction is only 0.9 day. Despite the potential for a surface source of CH_3CHO, this lifetime is significantly shorter than the timescale for mixing into the arctic free troposphere. Thus, mixing from surface sources should be discarded as an explanation for over an order magnitude model underestimation. Domine and Shepson (2002) also report an [HCHO]/[CH_3CHO] ratio of 2.5. However, the TOPSE observations show CH_3CHO mixing ratios consistently being larger than HCHO for all months and altitude ranges considered here. For example, a median [HCHO]/[CH_3CHO] ratio of 0.34 was observed for May conditions in the 3–6 km range. This behavior of CH_3CHO mixing ratios greater than HCHO mixing ratios does seem unusual given that typically lower molecular weight species are observed at higher mixing ratios than higher molecular weight analogs ($CH_4 > C_2H_6$, $CH_3OH > C_2H_5OH$). Given a lifetime for CH_3CHO of less than a day in May, the steady-state assumption for CH_3CHO should be a reasonable approximation. A simulation was performed to calculate the equivalent ethane-mixing ratio necessary to sustain CH_3CHO at 160 pptv for May conditions. An unrealistically large ethane-mixing ratio (40 ppbv) was necessary to photochemically sustain CH_3CHO at 160 pptv for May conditions. Cumulatively, these arguments shed uncertainty to the measurements of CH_3CHO during TOPSE. Interestingly, applying the ratio of [HCHO]/[CH_3CHO] observed by Domaine and Shepson to the HCHO observations yields CH_3CHO mixing ratio estimates (22 pptv for May, 3–6 km) closer to the model steady-state CH_3CHO mixing ratios (8 pptv for May, 3–6 km). Given these arguments, CH_3CHO was calculated to steady state in the model for the remainder of the NO_x budget results reported here.

3.3.3. In situ NO_x cycling with acetaldehyde calculated

Tables 4 and 5 presents the *net* NO_x fluxes due to PAN, HNO_3 and N_2O_5 in situ chemistry with CH_3CHO integrated to steady state and the odd nitrogen species constrained to their median measured mixing ratios. Since no direct measurement of HNO_4 was made during TOPSE, it is not possible to perform similar constrained calculations for HNO_4. Later, in Section 3.5, the role played by HNO_4 chemistry is highlighted with a series of time-dependent simulations.

HNO_3 is a *net* sink for NO_x throughout the arctic free troposphere between February and May. In the 3–6 km layer, the *net* NO_x sink due to HNO_3 formation varied from -0.5 to -4.4 pptv/day, increasing in magnitude in spring. Similarly, in the 1–3 km layer, the *net* NO_x sink due to HNO_3 formation varied from -0.1 to -7.0 pptv/day. *Net* NO_x loss rates to PAN show remarkable similarity to *net* NO_x loss rates to HNO_3 throughout the winter to spring transition in the 3–6 km range (Tables 4 and 5). Between 1 and 3 km, *net* NO_x loss to PAN is significantly larger than the *net* NO_x loss to HNO_3 for February conditions. For March and April, similar *net*

NO_x loss rates were calculated for both PAN and HNO_3. By May conditions, *net* NO_x loss to HNO_3 dominates over loss to PAN for 1–3 km. This difference in seasonal trend between 1–3 and 3–6 km is likely a reflection of the difference in the seasonal temperature dependence for the two altitude ranges. For 1–3 km, significant warming occurred by May conditions (266 K) resulting in a shorter thermal decomposition lifetime for PAN (10 days) which, in part, explains the smaller *net* NO_x loss rates to PAN compared to HNO_3. Seasonal changes in the $[NO_2]/[NO]$ ratio also shorten the effective lifetime of PAN for springtime conditions.

N_2O_5 is expected to have a lifetime less than 1 day in the arctic free troposphere. At warmer temperatures (>245 K), thermal decomposition is the favored loss mechanism, while at cooler temperatures hydrolysis is expected to dominate. N_2O_5 is a *net* sink for NO_x in the arctic free troposphere during the campaign; however, it behaves conversely to HNO_3 by decreasing in importance as a NO_x sink over the course of the winter–spring transition. N_2O_5 hydrolysis was included in the chemical mechanism as a heterogeneous reaction. Its rate depends critically on the aerosol surface area concentration and the N_2O_5 reactive uptake coefficient ($\gamma = 0.1$). Aerosol surface areas were estimated for this study from climatology generated using MOZART, a 3-D chemical transport model (Tie et al., 2003). These aerosol surface areas were recently evaluated in MOZART (Tie et al., 2001). Pseudo-first-order rate coefficients, k_{het}, varied between 10^{-4} and $10^{-5}\,s^{-1}$, generally increasing with season and decreasing with altitude in the arctic free troposphere. NO_x loss rates through N_2O_5 hydrolysis peaked at -2.9 pptv/day in the 3–6 km layer in February. In the 1–3 km layer, the NO_x loss rate peaked at -4.5 pptv/day in March. The increase in N_2O_5 hydrolysis between February and March for 1–3 km may stem from the change in median latitude between February (65°N) and March (74°N). These results show that N_2O_5 hydrolysis is the dominant loss process for NO_x under wintertime arctic conditions. By May, negligible NO_x loss rates due to N_2O_5 hydrolysis were calculated throughout the free troposphere due to lower modeled NO_3 mixing ratios and, thus, slower N_2O_5 production rates. These seasonal changes in NO_x loss through N_2O_5 are directly related to the availability of UV radiation to photolyze the intermediate NO_3 radical between February (mostly dark) to May conditions (mostly light). Since our calculation of *net* NO_x loss to N_2O_5 depends critically on aerosol surface area and these are non-measured parameters, two sensitivity simulations were performed for May conditions (58–85°N, 3–6 km) at five times greater/less than our estimates of aerosol surface area concentration. The results span the range from -3.4 to -0.90 pptv/day for February conditions (3–6 km). The smaller sensitivity with increases in aerosol concentration (-2.7 to -3.4 pptv/day) suggests that for arctic wintertime free troposphere conditions, air masses can saturate with regards to NO_x loss and further increases in aerosol surface area. The saturation point occurs when the rate of O_3 reaction with NO_2 becomes rate limiting compared to N_2O_5 hydrolysis. This effect has been studied in greater detail (Tie et al., 2003) and box model simulations show that for the wintertime arctic free troposphere the saturation point occurs at $\sim 10\,\mu m^2/cm^3$. This is of similar magnitude to the aerosol surface areas considered here, thus NO_x loss estimates are sensitive to decreases in aerosol surface areas, however insensitive to further aerosol surface area increases.

3.4. NO_y deficit and its seasonal dependence

Another intriguing observation from Fig. 2 is a seasonal dependence to the NO_y balance (defined here as (NO_y)–(PAN)–(PPN)–(HNO_3)–$(RONO_2)$–(NO_x)), which is a small deficit for February and systematically decreases to near balance in May for the 3–6 km layer and a small surplus in May for the 1–3 km layer. Limits for the mean NO_y balance in Fig. 2 are measurement uncertainties added in quadrature. Since NO_y is composed largely of PAN, then it should be noted that uncertainties in the NO_y balance stem largely from the uncertainties in the NO_y and PAN measurements. The NO_y budget is in near balance for all months with the exception of February (3–6 km) where the NO_y balance is significantly larger than zero when considering the combined measurement uncertainty (mean 60 ± 42 pptv). This is a positive result suggesting we can account for a large fraction (generally greater than 90%) of the observed NO_y. This is similar agreement to the NO_y balance observed for the recent SONEX campaign (Talbot et al., 1999).

Table 3 lists the median NO_y balance for February conditions. These observations support missing NO_y species in the range 20–100 pptv for February conditions (3–6 km). A linear fit of mean NO_y deficit vs. mean day of year for the data in Fig. 2, weighted by the inverse of the squared measurement uncertainties, yields slopes of -0.88 ± 0.85 pptv/day (3–6 km) and -1.00 ± 0.73 pptv/day (1–3 km).

Thus, the observations do support a marginal seasonal trend from a small deficit to small surplus. Fig. 3 also illustrates how the NO_y deficit varies as a function of temperature, $j(O^1D)$ and sulfate aerosol concentration for all the data in the arctic free troposphere between 3 and 6 km. A weak negative dependence is observed for temperature, $j(O^1D)$, and sulfate aerosol concentration, although there is large atmospheric variability. One potentially important odd nitrogen species not considered in the NO_y deficit calculations above is HNO_4. In the next section, the seasonal dependence for our modeled steady-state HNO_4 mixing

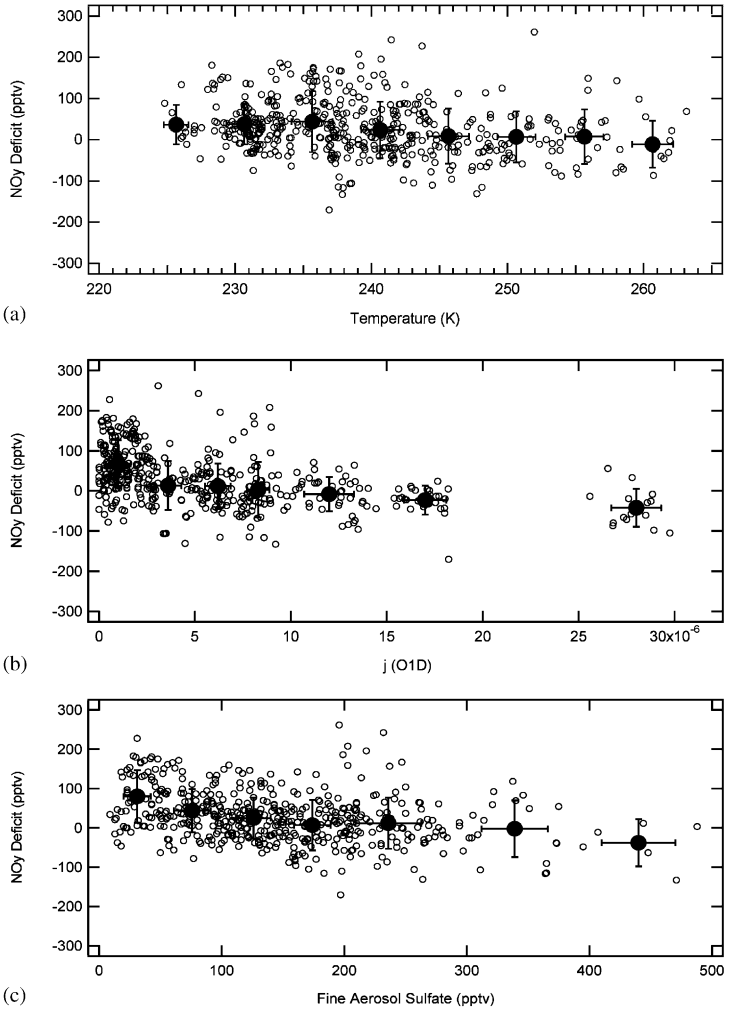

Fig. 3. The dependence of the observed NO_y deficit (defined as NO_y-PANs-HNO_3-NO_x) on temperature (panel a), O_3 photolysis frequency, $j(O^1D)$ (panel b), and fine aerosol sulfate (panel c) for the 3–6 km layer and between 58°N and 85°N.

ratio is calculated and compared to the seasonal trend in the observed NO_y balance.

3.5. Modeled HNO_4 chemistry

3.5.1. Lifetime considerations and steady-state HNO_4 mixing ratios

To calculate a steady-state HNO_4 and determine whether the steady-state assumption is reasonable, we performed four different time-dependent NO_x simulations where NO_x was initialized so that it decayed to its median measured mixing ratio in exactly 1–4 days (Figs. 4a and b, 3–6 km). In these simulations, HNO_4 mixing ratios were initialized at zero and hydrocarbons, CH_4, CO, H_2O, and O_3 were constrained at their median measured mixing ratios. CH_3CHO was initialized at its predetermined steady-state value and calculated during the simulation. In Fig. 4, the time axis is plotted such that model time = 0 corresponds to the point where model NO_x decayed to its median measured value. By comparing the HNO_4 at $t = 0$, we can estimate how long an air mass has to remain under these environmental conditions (i.e. temperature) for HNO_4 to reach steady state. For February conditions, the time for HNO_4 to reach steady-state is 3 days with a corresponding $(HNO_4)_{ss} = 40$ pptv (panel a and b). This relatively short induction time suggests that away from immediate NO_x sources (e.g. aircraft exhaust, fresh convection) HNO_4 will be in steady state with NO_x. The calculated steady-state methyl peroxynitrate ($CH_3O_2NO_2$) mixing ratio was 5 pptv, suggesting the organic homologues play a minor role in the NO_y budget compared to HNO_4.

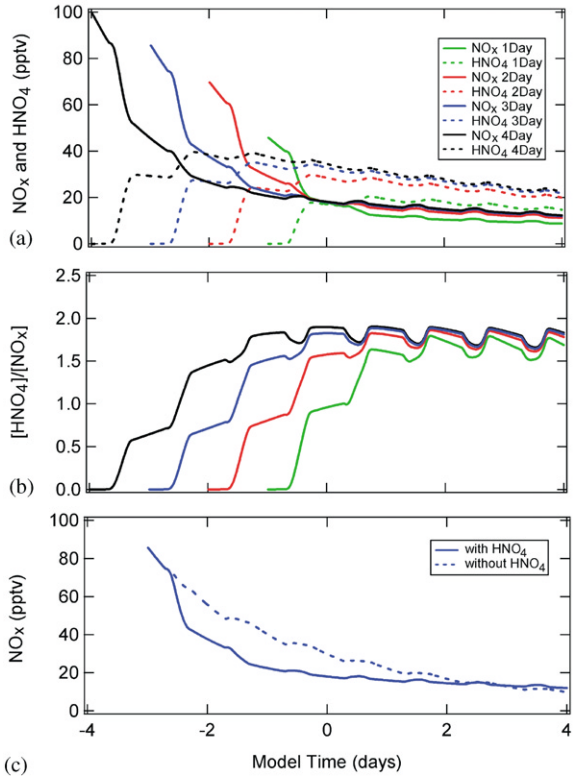

Fig. 4. Results of a time-dependent NO_x simulation where model NO_x decayed to its measured median mixing ratio in 1, 2, 3 and 4 days (panels a and b). Conditions are representative of February, 3–6 km and 58–85°N. Panel c includes the results for two simulations each initialized with the same NO_x mixing ratio, however one simulation run with and one without HNO_4 chemistry. Model run at observed median latitude of 64°N.

Other modeled NO_y species (HONO, N_2O_5 and NO_3) were also at negligible concentrations compared to NO_y; although it should be noted that the odd nitrogen flux through these species can be significant under cold, low light conditions. For the 1–3 km layer in the arctic, steady-state model HNO_4 was <5 pptv throughout the campaign.

An interesting paradox occurs when we compare the predicted steady-state HNO_4 mixing ratios with the median NO_y balance for May. For the median NO_x mixing ratio of 30 pptv (May, 3–6 km, 58–85°N) and $T = 243$ K, the model calculates a steady-state HNO_4 mixing ratio of 60 pptv. The steady-state assumption is surely valid for May conditions, as the induction time to reach steady state is less than a day. However, in comparing to the observed NO_y remainder in May (3–6 km), there is no room in the budget for a 60 pptv missing species. Furthermore, the increase in HNO_4 from 40 to 60 pptv is opposite to the seasonal trend in the NO_y balance. This suggests that there may be other unknown loss processes for HNO_4 in the spring. Recent laboratory studies show that HNO_4 can initiate the oxidation of S(IV) in aqueous particles (Amels et al., 1996; Warneck, 1999). HNO_4 is also known to react with HNO_2 (Logager and Sehested, 1993) and halide ions (Regimbal and Mozurkewich, 1997) in solution.

Murphy et al. (2002) discuss the temperature dependence of their indirect measurement of $[HNO_4]+[RO_2NO_2]$ during TOPSE. In their analysis, $[HNO_4]+[RO_2NO_2]$ is inferred as the difference between the measured sum of the peroxynitrates and the measured PANs, where they measured the sum of the peroxynitrates using a thermal dissociation laser-induced fluorescence technique. An even larger temperature dependence was observed for their inferred $[HNO_4]+[RO_2NO_2]$ mixing ratios with estimates of ~ 100 pptv at $T < 240$ K. These results clearly support the need for direct measurements of HNO_4 of sufficient precision and accuracy along with heterogeneous chemical modeling studies to shed further light on this apparent paradox in the NO_y balance.

3.5.2. *HNO_4 and its impact on the NO_x lifetime*

Since our modeling calculations and the measurements of Murphy suggest that HNO_4 can be a significant fraction of NO_y in winter and there is some marginal evidence for an NO_y deficit in winter, it is useful to study the role played by HNO_4 in the NO_x budget in the arctic wintertime. Fig. 4c compares NO_x decays for two simulations with and without HNO_4 chemistry. The solid curve is identical to the solid blue curve shown in Fig. 4a for the model simulation with a 3-day induction time and HNO_4 chemistry included. The dashed line in Fig. 4c is the corresponding NO_x decay for a simulation with identical initial NO_x, however no HNO_4 chemistry. The importance of HNO_4 to modeled NO_x mixing ratios depends on the age of the NO_x in the air mass. For 'fresh' air masses, NO_x decays more quickly with the HNO_4 chemistry included due to the initial formation of HNO_4. However, for more 'aged' air masses, the HNO_4 reservoir acts as a buffer replenishing NO_x. The cross-over point where the addition of HNO_4 chemistry enhances NO_x mixing ratios over the case with no HNO_4 chemistry occurs between 5 and 6 days and is largely independent of initial NO_x mixing ratios. It is very likely that typical air masses sampled in the arctic free troposphere have NO_x ages longer than 5–6 days and thus the presence of the HNO_4 reservoir can act as a source for NO_x in the arctic. Here we considered a constant temperature history for the modeled air mass at the observed median temperature (February, 3–6 km). Given that thermal decomposition is the dominant loss process for HNO_4, the cross-over point will be a strong function of the temperature history of an air mass.

To further quantify the role played by HNO_4 in the NO_x budget, we calculated diurnally averaged *net* NO_x

Table 6
24-h average NO_x budget in the arctic free troposphere due to reservoir cycling (3–6 km) derived from a time-dependent simulation with CH_3CHO calculated (in pptv/day)

Reactions considered	February 0–1 day	February 4–5 day	May 0–1 day	May 4–5 day
$OH + NO_2 \rightarrow HNO_3$ $HNO_3 + OH \rightarrow H_2O + NO_3$ $HNO_3 + h\nu \rightarrow OH + NO_2$	−3.0	−0.3	−20.9	−3.9
$CH_3CO_3 + NO_2 \rightarrow PAN$ $PAN + M \rightarrow CH_3CO_3 + NO_2$ $PAN + h\nu \rightarrow CH_3CO_3 + NO_2$	−0.7	−0.5	−4.4	−3.4
$NO_2 + NO_3 \rightarrow N_2O_5$ $N_2O_5 + M \rightarrow NO_2 + NO_3$ $N_2O_5 + h\nu \rightarrow NO_2 + NO_3$	−16.4	−2.7	−0.29	−0.03
$HO_2 + NO_2 \rightarrow HNO_4$ $HNO_4 + h\nu \rightarrow NO_2 + HO_2$ $HNO_4 + M \rightarrow NO_2 + HO_2$	−28.4	+3.4	−69.3	+5.4

Calculated for 0–1 day and 4–5 day of a box model simulation where NO_x decreased to its median measured mixing ratio by the end of the 4th day. Other NO_y species were initialized at their measured medians and not constrained. Model CH_3CHO was initialized at model steady-state mixing ratio (from a prior determined simulation) and calculated. Model run at observed monthly median latitudes of 64°N and 73°N for February and May conditions, respectively.

loss/production rates from a time-dependent NO_x simulation for February in the arctic mid-troposphere (February simulation the same as in Fig. 4; analogous simulation for May also performed). If we look at the diurnally averaged *net* NO_x rates for the first 24 h of these simulations we find significant *net* NO_x loss rates to HNO_4 (−28 and −69 pptv/day for February and May) compared to the other odd nitrogen reservoirs (Table 6). Conversely, if we arbitrarily look at the model simulations for a more 'aged' air mass, after 4 days, we find that HNO_4 is a *net* source for NO_x (+3.4 and +5.4 pptv/day for February and May) largely countering the *net* NO_x losses to N_2O_5, PAN and HNO_3. These results yield a consistent picture with Tables 4 and 5 for N_2O_5, PAN and HNO_3 and now show the additional role played by HNO_4. For 'fresh' air masses, HNO_4 is a *net* sink for NO_x. For more 'aged' air masses, HNO_4 is a *net* source for NO_x, largely countering the NO_x losses to N_2O_5 in the winter and PAN and HNO_3 in the spring.

3.5.3. *HNO_4 and its impact on O_3 production*

The time evolution of modeled O_3 mixing ratios for the two scenarios discussed in the prior section (with and without HNO_4 chemistry) was also considered. The goal of these simulations was to evaluate the importance of HNO_4 chemistry on the amount of O_3 produced along a trajectory from a source region for NO_x. The initial production of HNO_4 near NO_x sources clearly slows the rate of O_3 production (after 5 days O_3 difference was 0.7 ppbv for February conditions). For more 'aged' air masses, the buffering impact of HNO_4 begins to narrow the difference between the two O_3 traces, however even after 20 days the modeled O_3 from the simulation with HNO_4 chemistry included still has slightly smaller O_3 mixing ratios (difference of 0.4 ppbv). Qualitatively, similar results were obtained for a simulation in May with maximum differences in O_3 of 2.3 ppbv after 5 days and 0.9 ppbv after 20 days.

Thus, these simulations suggest that HNO_4 chemistry impacts the timing of O_3 production; however, the cumulative impact on O_3 mixing ratios after a 20-day trajectory is minimal.

4. Conclusions

In this paper, we evaluated the in situ recycling reactions for NO_x in the arctic free troposphere using a constrained box model. In the winter, N_2O_5 hydrolysis is the largest *net* sink for NO_x (−2.9 pptv/day in February); however, it reduces to negligible importance in spring due to the seasonal increase in the rate of NO_3 photolysis. NO_x loss through N_2O_5 is limited by the rate of the $NO_2 + O_3$ reaction for conditions in the wintertime arctic free troposphere. HNO_3 and PAN are also permanent *net* sinks for NO_x in the arctic free troposphere during TOPSE. Modeled CH_3CHO mixing ratios are an order of magnitude smaller than observations. Given our current understanding of atmospheric chemistry, constraining the model with observed CH_3CHO yields unrealistic estimates for *net* NO_x loss rates to PAN. Median observed CH_3CHO mixing ratios

were also larger than observed HCHO mixing ratios for arctic free troposphere cases; a rather unusual behavior. Thus, until the CH_3CHO canister measurements are fully characterized in the laboratory and formally intercompared in the field, the TOPSE CH_3CHO observations are considered preliminary and suspect. Using simulations where CH_3CHO reached steady state, the *net* NO_x loss to PAN was calculated to be of comparable magnitude to *net* NO_x loss to HNO_3, with *net* PAN formation being larger in the wintertime lower free troposphere and *net* HNO_3 formation being larger in the springtime lower free troposphere. Overall, NO_x loss due to N_2O_5 hydrolysis dominates in winter, whereas NO_x loss due to PAN and HNO_3 formation dominates in the spring. These conclusions derived from an observationally constrained box model with explicit chemistry will be useful in future validation of NO_x loss processes in 3D chemical-transport models.

The role of HNO_4 chemistry in impacting arctic free troposphere NO_x mixing ratios depends on the age of the air mass. Near NO_x sources, HNO_4 is a net sink for NO_x; however, HNO_4 decomposition and IR photolysis can be *net* sources of NO_x for more 'aged' arctic air masses. Model simulations suggest the cross-over point to NO_x enhancement due to the buffering impact of HNO_4 occurs after 5–6 days (dependent of temperature history of air mass). Given that the age of NO_x in typical arctic free troposphere air samples is likely older than 5–6 days, HNO_4 chemistry tends to enhance remote NO_x mixing ratios. These conclusions may change as our understanding of the HNO_4 heterogeneous chemistry improves in the future. While the presence of HNO_4 chemistry may *locally* enhance O_3 production rates for 'aged' air masses, the impact of HNO_4 over the entire air parcel trajectory is a slight decrease in O_3 mixing ratio.

The NO_y budget is in near balance for all months with the exception of February (3–6 km) where a mean deficit of 60 ± 42 pptv is observed. Thus, it is possible for the observed NO_y deficit to support the modeled HNO_4 mixing ratio of 40 pptv in February (3–6 km). It is intriguing that the marginal seasonal trend in the NO_y balance from small deficit to small surplus is not consistent with the seasonal trend in our modeled HNO_4 mixing ratios. The modeled HNO_4 of 60 pptv in May (3–6 km) is only supported if we consider the upper limits for the combined measurement uncertainties, -18 ± 75 pptv. Thus, it is speculated that unknown HNO_4 chemistry may be important in the arctic springtime. Future measurements of HNO_4 in combination with modeling studies that incorporate heterogeneous laboratory studies are clearly warranted.

Finally, these observations and modeling results illustrate how NO_x can accumulate as the PAN reservoir during the spring months in the northern free troposphere. As a result, air masses leaving the high latitude arctic free troposphere and following anti-cyclonic, descending trajectories will have high rates of PAN thermal decomposition, which can enhance O_3 production rates at impacted mid-latitude surface locations.

Acknowledgements

C.S. would like to thank the Advanced Study Program within the National Center for Atmospheric Research for a fellowship. NCAR is sponsored by the National Science Foundation and operated by the University Corporation for Atmospheric Research. D.B., B.H., and R.T. appreciate support from the Atmospheric Sciences Division and the Office of Polar Programs of the National Science Foundation. The authors are also grateful to NCAR's Research Aviation Facility for their commitment to the TOPSE mission.

References

Amels, P., Elias, H., Gotz, U., Steingens, U., Wannaowius, K.J., 1996. Kinetic investigation of the stability of peroxynitric acid and of its reaction with sulfur (IV) in aqueous solution. In: Warneck, P. (Ed.), Heterogeneous and Liquid Phase Processes, Transport and Chemical Transformations of Pollutants in the Troposphere, Vol. 2. Springer, New York, pp. 77–88.

Atkinson, R., 1994. Gas-phase tropospheric chemistry of organic-compounds. Journal of Physical and Chemical Reference Data R1-&.

Atkinson, R., 1997a. Atmospheric reactions of alkoxy and ß-hydroxyalkoxy radicals. International Journal of Chemical Kinetics 29, 99–111.

Atkinson, R., 1997b. Gas-phase tropospheric chemistry of volatile organic compounds. 1. Alkanes and alkenes. Journal of Physical and Chemical Reference Data 26 (2), 215–1290.

Atkinson, R., Baulch, D.L., Cox, R.A., Hampson, R.F., Kerr, J.A., Rossi, M.J., Troe, J., 2000. Evaluated kinetic and photochemical data for atmospheric chemistry: supplement VIII, halogen species—IUPAC subcommittee on gas kinetic data evaluation for atmospheric chemistry. Journal of Physical and Chemical Reference Data 29 (2), 167–266.

Atlas, E.L., et al., 1992. Partitioning and budget of NO_y species during MLOPLEX. Journal of Geophysical Research 97, 10449–10462.

Atlas, E.L., Ridley, B.A., Cantrell, C.A., 2003. The tropospheric ozone production about the spring equinox (TOPSE) experiment: introduction. Journal of Geophysical Research 108 (D4), 10.1029/2002JD003172.

Beine, H.J., Engardt, M., Jaffe, D.A., Hov, O., Holmen, K., Stordal, F., 1996. Measurements of NO_x and aerosol particles at the NY-Alesund Zeppelin mountain station on Svalbard: influence of regional and local pollution sources. Atmospheric Environment 30, 1067–1079.

Beine, H.J., et al., 1997. High-latitude springtime photochemistry. 1. NO_x, PAN and ozone relationships. Journal of Atmospheric Chemistry 27 (2), 127–153.

Chameides, W., Walker, J.C.G., 1973. Photochemical theory of tropospheric ozone. Transactions of the American Geophysical Union 54 (12), 1293–1293.

Christensen, L.E., Okumura, M., Sander, S.P., Salawitch, R.J., Toon, G.C., Sen, B., Blavier, J.-F., Jucks, K.W., 2002. Kinetics of $HO_2 + HO_2 = H_2O_2 + O_2$: implications for stratospheric H_2O_2. Geophysical Research Letters 29.

Crosley, D.R., 1996. NO_y blue ribbon panel. Journal of Geophysical Research 101, 2049–2052.

Crutzen, P.J., 1974. Photochemical reaction initiated by and influencing ozone in unpolluted tropospheric air. Tellus 26, 45–55.

Crutzen, P.J., 1979. The role of NO and NO_2 in the chemistry of the troposphere and stratosphere. Annual Review of Earth and Planetary Science 7, 443–472.

Demore, W.B., 1997. Chemical kinetics and photochemical data for use in stratospheric modeling. JPL Publications 97-4.

Demore, W.B., 2000. Chemical kinetics and photochemical data for use in stratospheric modeling, JPL Publications.

Domine, F., Shepson, P.B., 2002. Air-snow interactions and atmospheric chemistry. Science 297, 1506–1510.

Hamlin, A.J., Honrath, R., 2002. A modeling study of the impacts of winter–spring arctic outflow on the NO_x and O_3 budget of the North Atlantic troposphere. Journal of Geophysical Research 107, 2001JD000453.

Jacob, D.J., Heikes, B.G., Fan, S.M., Logan, J.A., Mauzerall, D.L., Bradshaw, J.D., Singh, H.B., Gregory, G.L., Talbot, R.W., Blake, D.R., Sachse, G.W., 1996. Origin of ozone and NO_x in the tropical troposphere: a photochemical analysis of aircraft observations over the south Atlantic basin. Jouranal of Geophysical Research 101 (D19), 24235–24250.

Jaegle, L., Jacob, D.J., Brune, W.H., Faloona, I., Tan, D., Heikes, B.G., Kondo, Y., Sachse, G.W., Anderson, B., Gregory, G.L., Singh, H.B., Pueschel, R., Ferry, G., Blake, D.R., Shetter, R.E., 2000. Photochemistry of HO_x in the upper troposphere at northern midlatitudes. Journal of Geophysical Research 105 (D3), 3877–3892.

Kondo, Y.S., et al., 1997. Profiles and partitioning of reactive nitrogen over the Pacific Ocean in winter and early spring. Journal of Geophysical Research 102, 28405–28424.

Kotchenruther, R.A., Jaffe, D.A., Jaegle, L., 2001. Ozone photochemistry and the role of peroxyacetyl nitrate in the springtime northeastern pacific troposphere: results from the photochemical ozone budget of the eastern north pacific atmosphere (phobea) campaign. Journal of Geophysical Research 106 (D22), 28731–28742.

Levy II, H., 1972. Photochemistry of the lower troposphere. Planetary and Space Science 20, 919–935.

Levy II, H., Moxim, W.J., Klonecki, A.A., Kasibhatla, P.S., 1999. Simulated tropospheric NO_x: its evaluation, global distribution and individual source contributions. Journal of Geophysical Research 104, 26279–26306.

Logager, T., Sehested, K., 1993. Formation and decay for peroxynitric acid—a pulse-radiolysis study. Journal of Physical Chemistry 97 (39), 10047–10052.

Madronich, S., Calvert, J.G., 1990. Permutation reactions of organic peroxy-radicals in the troposphere. Journal of Geophysical Research 95 (D5), 5697–5715.

Madronich, S., Flocke, S., 1998. The role of solar radiation in atmospheric chemistry. In: Boule, P. (Ed.), Handbook of Environmental Chemistry. Springer, Heidelberg, pp. 1–26.

Mereau, R., Rayez, M.T., Caralp, F., Rayez, J.C., 2000. Theoretical study of alkoxyl radical decomposition reactions: structure-activity relationships. Physical Chemistry and Chemical Physics 2 (17), 3765–3772.

Moxim, W.J., Levy II, H., Kasibhatla, P.S., 1996. Simulated global tropospheric pan: its transport and impact on NO_x. Journal of Geophysical Research 101, 12621–12638.

Murphy, et al., 2002. Measurements of the sum of HO_2NO_2 and $CH_3O_2NO_2$ in the remote troposphere, Journal of Geophysical Reserach, submitted for publication.

Orlando, J.J., Tyndall, G.S., Bilde, M., Ferronato, C., Wallington, T.J., Vereecken, L., Peeters, J., 1998. Laboratory and theoretical study of the oxy radicals in the OH- and Cl-initiated oxidation of ethene. Journal of Physical Chemistry A 102, 8116–8123.

Parrish, D.D., et al., 1993. The total reactive oxidized nitrogen levels and the partitioning between the individual species at six rural sites in eastern North America. Journal of Geophysical Research 98, 2927–2939.

Regimbal, J.M., Mozurkewich, M., 1997. Peroxynitric acid decay mechanisms and kinetics at low pH. Journal of Physical Chemistry A 101, 8822–8829.

Ridley, B.A., et al., 1991. Recent measurements of oxidized nitrogen compounds in the troposphere. Atmospheric Environment 25, 1905–1926.

Roberts, J.M., 1990. The atmospheric chemistry of organic nitrates. Atmospheric Environment 24A (2), 243–287.

Roberts, J.M., Flocke, F., Stroud, C.A., Hereid, D., Williams, E.J., Fehsenfeld, F.C., Brune, W., Martinez, M., Harder, H., 2002. Ground-based measurements of PANs during the 1999 southern oxidant STUDY Nashville Intensive. Journal of Geophysical Research 107, 10.1029/2001JD000947.

Roehl, C.M., Nizkorodov, S.A., Zhang, H., Blake, G.A., Wennberg, P., 2002. Photodissociation of peroxynitric acid in the near-IR. Journal of Physical Chemistry 106, 3766–3772.

Sandholm, S., et al., 1994. Summertime partitioning and budget of NO_y compounds in the troposphere over Alaska and Canada: Able 3B. Journal of Geophysical Research 99, 1837–1861.

Schultz, M., 1999. On the origin of tropospheric ozone and NO_x over the tropical South Pacific. Journal of Geophysical Research 104, 5829–5843.

Schultz, M.G., Jacob, D.J., Bradshaw, J.B., Sandholm, S.T., Dibb, J.E., Talbot, R.W., Singh, H.B., 2000. Chemical NO_x budget in the upper troposphere over the tropical South Pacific. Journal of Geophysical Research 105, 6669–6679.

Singh, H., Chen, Y., Staudt, A., Jacob, D., Blake, D., Heikes, B., Snow, J., 2001. Evidence from the pacific troposphere for large global sources of oxygenated organic compounds. Nature 410, 1078–1081.

Stroud, C.A., et al., 2003. Photochemistry in the arctic free troposphere: ozone budget and its dependence on nitrogen oxides and the production rate of free radicals. Journal of Atmospheric Chemistry, submitted for publication.

Talbot, R.W., et al., 1999. Reactive nitrogen budget during the NASA SONEX mission. Journal of Geophysical Research 26, 3057–3060.

Tie, X., Brasseur, G., Emmons, L., Horowitz, L., Kinnison, D., 2001. Effects of aerosols on tropospheric oxidants: a global model study. Journal of Geophysical Research 106 (D19), 22931–22964.

Tie, X.X., Emmons, L., Horowitz, L., Brasseur, G., Ridley, B., Atlas, E., Stround, C., Hess, P., Klonecki, A., Madronich, S., Talbot, R., Dibb, J., 2003. Effect of sulfate aerosol on tropospheric NO_x and ozone budgets: model simulations and TOPSE evidence. Journal of Geophysical Research 108 (D4), 8364.

Tyndall, G.S., Cox, R.A., Granier, C., Lesclaux, R., Moortgat, G.K., Pilling, M.J., Ravishankara, A.R., Wallington, T.J., 2001. Atmospheric chemistry of small organic peroxy radicals. Journal of Geophysical Research 106 (D11), 12157–12182.

Warneck, P., 1999. The relative importance of various pathways for the oxidation of surfur dioxide and nitrogen oxides in sunlit continental fair weather cloud. Physical Chemistry and Chemical Physics 1, 5471–5483.